Orientation of the Tyrosyl D, Pheophytin Anion, and Semiquinone $Q_A^{\bullet -}$ Radicals in Photosystem II Determined by High-Field Electron Paramagnetic Resonance†

Pierre Dorlet, A. William Rutherford, and Sun Un*

Section de Bioénergétique, Département de Biologie Cellulaire et Moléculaire, CNRS URA 2096, CEA Saclay, F-91191 Gif-sur-Yvette Cedex, France

Received January 31, 2000; Revised Manuscript Received April 20, 2000

ABSTRACT: The radical forms of two cofactors and an amino acid in the photosystem II (PS II) reaction center were studied by using high-field EPR both in frozen solution and in oriented multilayers. Their orientation with respect to the membrane was determined by using one-dimensionally oriented samples. The ring plane of the stable tyrosyl radical, $Y_D^{\bullet}$, makes an angle of 64° ± 5° with the membrane plane, and the C−O direction is tilted by 72° ± 5° in the plane of the radical compared to the membrane plane. The semiquinone, $Q_A^{\bullet -}$, generated by chemical reduction in samples lacking the non-heme iron, has its ring plane at an angle of 72° ± 5° to the membrane plane, and the O−O axis is tilted by 21° ± 5° in the plane of the quinone compared to the membrane plane. This orientation is similar to that of $Q_A^{\bullet -}$ in purple bacteria reaction centers except for the tilt angle which is slightly bigger. The pheophytin anion was generated by photoaccumulation under reducing conditions. Its ring plane is almost perpendicular to the membrane with an angle of 70° ± 5° with respect to the membrane plane. This is very similar to the orientation of the pheophytin in purple bacteria reaction centers. The position of the *g* tensor with respect to the molecule is tentatively assigned for the anion radical on the basis of this comparison. In this work, the treatment of orientation data from EPR spectroscopy applied to one-dimensionally oriented multilayers is examined in detail, and improvements over previous approaches are given.

Photosystem II (PS II)[1] is a large membrane protein composed of several intrinsic and extrinsic subunits. It catalyzes the oxidation of water into dioxygen and the reduction of quinones (*1*−*4*). These processes result from a charge separation initiated by photoexcitation of a chlorophyll species, P_{680}, which forms a highly reducing singlet state. An electron is then given to a pheophytin *a* molecule and subsequently transferred to a plastoquinone molecule, Q_A, forming the semiquinone radical, while the P_{680}^+ species is reduced by a redox-active tyrosine, Y_Z.

Under normal conditions, the semiquinone radical is magnetically coupled to a high-spin non-heme Fe^{2+} (*5*−*7*). It is, however, possible to decouple the two species by a range of different biochemical methods: pH 11 treatment (*8*), conversion of the Fe^{2+} to the low-spin $S = 0$ state by cyanide treatment (*9*), substitution by Zn^{2+} (*10*), and removal of the non-heme iron (*11*). In these treated preparations, the addition of a chemical reductant in the dark allows the direct observation of the semiquinone radical EPR signal. Under strongly reducing conditions, it is possible to doubly reduce the quinone Q_A to the quinol form by continuous illumination above 273 K (*12*). It is then possible to photoaccumulate the pheophytin anion radical (*13*−*15*). In the absence of chemical reductant, another radical, the stable tyrosyl radical, $Y_D^{\bullet}$, is present in the dark. This species plays a role in electron transfer reactions under certain conditions and is symmetrically related (*16*) to the kinetically competent tyrosyl radical, $Y_Z^{\bullet}$, which is involved in oxygen evolution.

Crystallographic data on PS II are limited to an electron crystallographic structure with a resolution of 8 Å (*17*). This resolution is insufficient to determine the position of the electron transfer components apart from chlorophyll molecules. However, a fairly detailed structural model has evolved for the main aspects of the PS II reaction center based on comparative spectroscopic measurements on PS II and purple bacteria reaction centers (*18*), amino acid sequence comparisons (*19*), site-directed mutagenesis (*20*, *21*), biochemical studies (*22*), and computer modeling (*23*, *24*). Spectroscopic approaches, particularly EPR, have provided specific structural information which is gradually replacing the assumptions in the model (*16*, *25*−*31*).

By using the inherent high resolution of high-field EPR in combination with 1D-oriented samples, it is possible to determine directly the orientation of a radical with respect to the axis of orientation. This method has been applied successfully for $Y_D^{\bullet}$ (*30*). Here we present data with improved resolution for this radical both in frozen solution

† This work was supported by grants from the Human Frontiers Science Organization (Contract RGO349), from the EU through HCM Grants FMRX-CT98-0214 and FMRX-CT96-0031, and from the Region Ile-de-France (Contract Sesame). P.D. was supported by a fellowship from the CEA.

* Corresponding author. Fax: 33 (0)1 69 08 87 17. E-mail: sun@ozias.saclay.cea.fr.

[1] Abbreviations: PS II, photosystem II; $Y_D^{\bullet}$, stable tyrosyl radical in PS II; Pheo, the pheophytin electron acceptor; Q_A, the primary electron acceptor of the iron−quinone complex; EPR, electron paramagnetic resonance; ESEEM, electron spin−echo envelope modulation; ENDOR, electron nuclear double resonance; MES, 2-(*N*-morpholino)-ethanesulfonic acid; EDTA, ethylenediaminetetraacetic acid.

10.1021/bi000175l CCC: $19.00
Published on Web 06/06/2000

and oriented samples (a preliminary account of this work for the orientation of the tyrosyl radical has been presented in ref *30b*). We also present high-field EPR spectra of $Q_A^{\bullet-}$ and the pheophytin anion radical which were generated under reducing conditions in PS II samples pretreated at pH 11 to remove the non-heme iron. By using oriented samples, the orientations of these cofactors were also determined. The results are compared with structural data from bacterial reaction centers.

MATERIALS AND METHODS

Sample Preparation. All biochemical preparations were performed on ice under dim green light unless otherwise stated. Photosystem II membranes were prepared according to the procedure described previously (*32*). The preparations were frozen at a chlorophyll concentration of about 8 mg of Chl/mL in SMN buffer (sucrose, 0.4 M, MES, 50 mM, pH 6.0, and NaCl, 15 mM) and stored at −80 °C until used.

Mn depletion was performed by exposing the PS II membranes (0.5 mg of Chl/mL) to room light in a 0.8 M Tris buffer, pH 8.0, for 20 min, followed by two washes in the dark with a 50 mM MES, pH 6.0, and 1 mM EDTA buffer and resuspension in SMN buffer. This treatment also results in the loss of the 17, 24, and 33 kDa extrinsic polypeptides of PS II.

Removal of the non-heme iron was based on the procedure in ref *8*. Tris-washed PS II membranes were incubated for 10 min at room temperature in complete darkness in 50 mM glycine, pH 11.0, 0.4 M sucrose, 10 mM NaCl, and 1 mM EDTA. They were then pelleted and washed once with a pH 9.0 glycine buffer.

To generate the semiquinone $Q_A^{\bullet-}$ radical, the membranes were chemically reduced in complete darkness by one wash (suspension in buffer for 5 min followed by centrifugation for 20 min) with pH 9.0 glycine buffer poised at −450 mV with sodium dithionite and resuspension in the same buffer. This treatment eliminates the $Y_D^{\bullet}$ radical. The pheophytin radical was induced by illuminating the reduced membranes at 288 K for 12 min. This treatment eliminates the semiquinone by causing its double reduction (*12*). No redox mediators were used. The redox potential was adjusted with sodium dithionite under anaerobic conditions and was measured with a platinum electrode and a calomel reference electrode. Measured redox potentials were normalized to the standard hydrogen electrode by calibrating the electrode with a saturated quinhydrone solution (potential 286 mV at pH 6.5).

To prepare the oriented samples, the pretreated PS II membrane preparation was painted onto plastic films (3M transparency film, no. PP2500) and dried in a 90% humidity atmosphere in darkness at 4 °C. In this work, EPR spectra were recorded for two different orientations of the plastic films with respect to the magnetic field. The plastic sheets were mounted perpendicular and parallel to the magnetic field (which is vertical in our setup) in two separate tubes. For the orientation corresponding to the magnetic field perpendicular to the film normal, the plastic strips, measuring 20 mm by 2.5 mm, were put into regular quartz EPR tubes. For the orientation corresponding to the magnetic field perpendicular to the films, small plastic squares (5 mm by 5 mm) were stacked horizontally in a polycarbonate tube which was used as the sample holder. For the determination of the orientation of the quinone and the pheophytin, the prereduced samples were dried on the plastic films under anaerobic conditions. The films were then inserted in the tubes and submerged in a pH 9.0 glycine-buffered dithionite solution which was subsequently frozen in the dark. After determination of the orientation of the semiquinone radical, the samples were brought to 288 K under anaerobic conditions and illuminated for 12 min at the same temperature to induce the pheophytin anion radical.

EPR Spectroscopy. Nine GHz EPR spectra were recorded with a TE_{102} mode cavity at liquid helium temperatures on a Bruker ESP 300 spectrometer equipped with a liquid helium continuous-flow cryostat and transfer line from Oxford Instruments. The microwave frequency was measured with a Hewlett-Packard 5350B frequency counter connected to the microwave bridge.

Two hundred eighty five GHz EPR spectra were recorded on a lab-built transmission spectrometer, the principles of which are similar to those described by Muller et al. (*33*). In this case, however, a synthesizer source (ELVA-1, Saint Petersbourg, Russia) capable of generating a minimum output power of 100 mW over a 93−97 GHz frequency range was used as the fundamental microwave source. In conjunction with the synthesizer, frequency doubler and tripler (Radiometric Physics, Menkenheim, Germany) were used to work in the 186−194 GHz and 279−291 GHz frequency ranges (the final power output was 3−4 mW). The signal was detected by using an InSb bolometer (QMC Instruments Ltd., London, England) in conjunction with a lock-in amplifier (SRS, Sunnyvale, CA) and field modulation. The amplitude of the modulation field was calibrated by using a standard sample. The magnetic field was generated by using a superconducting 10.5 T magnet (Oxford Instruments, Oxon, England). The value of the magnetic field was obtained from the magnet power supply with a manufacturer-specified accuracy of ±0.05 mT. The absolute magnetic field was calibrated by using a manganese-doped magnesium oxide standard (*34*). Under conditions with which the data were recorded, the absolute error in g was 10^{-4}. However, the relative accuracy (difference between two data points of a given spectrum) was better than 2×10^{-5} in g. Sample temperature regulation was achieved by using a built-in helium flow cryostat.

Simulations of the Data. The powder spectra were obtained by calculating the resonant field for 10^6 random orientations of the applied magnetic field with respect to the g axis frame and summing the results. The transition probability was taken to be unity. Except for the spectra of the tyrosyl radical in frozen solution, no hyperfine couplings were included because they were unresolved and contribute only to the line width of the experimental spectra. The resulting orientation-integrated spectra were convoluted with a derivative Gaussian line shape with a suitable line width. Fitting parameters were estimated by nonlinear minimization of the root-mean-square (rms) difference between the experimental and calculated spectra using a standard conjugate gradient method (*35*). Gaussian distributions were obtained by the method of normal deviates (*35*). All calculations were performed on a Digital Equipment Corporation workstation by using local programs written in Fortran 77.

Scheme 1: Schematic Representation of a Protein Embedded in a Membrane Oriented on a Plastic Film[a]

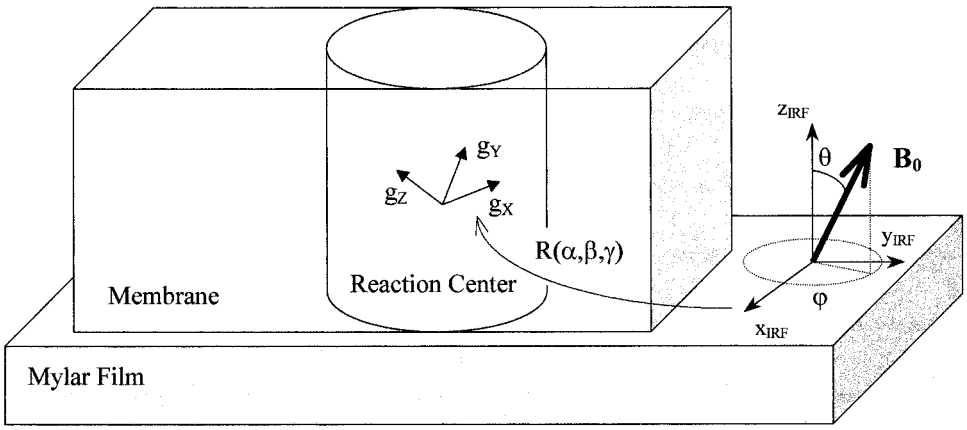

[a]The intermediary reference frame (IRF) is linked to the film. The applied magnetic field is expressed in the IRF by using the polar angles (θ, φ). The IRF is related to the g axis frame by the rotation R (α, β, γ).

Theory of EPR for 1D-Oriented Samples. To calculate the resonance field of a spin, the orientation of the magnetic field with respect to the g axis system must be known. This orientation is specified by two angles. For powder samples, these angles will take on all possible values. For 1D-oriented samples, their values will be restricted and will depend on the direction of the sample orientation. To facilitate the calculation of spectra of 1D-oriented samples, an intermediate reference frame (IRF) was used (see Scheme 1). The IRF is linked to the plastic film. Its z axis is along the film perpendicular and also corresponds to the direction along which the protein complexes and membrane fragments are nominally ordered. The IRF x and y directions are perpendicular to z and have no physical significance. To calculate the orientation of the magnetic field with respect to the g axis system, the following transformation is used:

$$\mathbf{B}_{LAB} \xrightarrow{R(\theta,\varphi)} \mathbf{B}_{IRF} \xrightarrow{R(\alpha,\beta,\gamma)} \mathbf{B}_{GA}$$

where $\mathbf{B}_{LAB}$, $\mathbf{B}_{IRF}$, and $\mathbf{B}_{GA}$ are vectors of equal magnitude expressed in the laboratory, the intermediary reference, and the g axis frames, respectively, and R are rotation matrices which carry out the transformation between the different axis systems. The angles θ and φ define the orientation of the magnetic field in the IRF. The transformation between the IRF and the g axis system is given by three Euler angles: α, β, and γ (*36*). It is used to express the components of $\mathbf{B}_{IRF}$ in the g axis system. The IRF is rotated into the g axis system by a γ-rotation about z_{IRF} followed by a β-rotation about y_{IRF}, and finally an α-rotation about z_{IRF}. Orientation averaging was achieved by generating random orientations of the magnetic field in the (x, y) plane of the IRF (random φ angles) while the angle θ between the applied magnetic field and z_{IRF} was held constant. The averaging process, in effect, also averages all possible values of the Euler angle α, and therefore, the oriented spectra are independent of this angle. For an ideally oriented sample, z_{IRF} corresponds to the normal of the membrane plane; hence β and γ define the orientation of the g frame within the photosynthetic membrane. In this paper, the angles defining the orientation of the radicals within the membrane are reported as (β, γ) pairs. β is the angle between the g_z axis and the membrane normal, and γ is the angle between the g_x axis and the projection of the membrane normal on the (g_x, g_y) plane.

For these 1D-oriented samples, the angle θ between z_{IRF} and the applied magnetic field is fixed in the experiment. If the magnetic field is parallel to z_{IRF}, then θ is 0° and the g value for the resonance is independent of φ (and α). In this case, the EPR resonance field is only determined by β and γ; the spectrum is identical to that of a single crystal exhibiting a single line. When the magnetic field is perpendicular to z_{IRF}, θ is 90° and φ takes all possible values. For each value of φ, a different effective g value is obtained, resulting in a spectrum which is approximately the difference between the powder spectrum and the single crystal-like spectrum obtained when the magnetic field is parallel to z_{IRF} (see Figure 4).

The calculation of the spectra of 1D-oriented samples is determined by three independent angles, θ, β, and γ, and the g values of the radical. Uncertainty or error in positioning the films within the magnet corresponds to uncertainty or error in θ. A distribution in the g tensor orientation with respect to the normal of the plastic films naturally corresponds to a distribution in both β and γ. Such a distribution arises either from variation in the local membrane normal with respect to z_{IRF} (mosaic spread) or from the positional disorder of the radical within the protein. We have modeled this distribution with Gaussian functions, the widths of which were adjusted to fit the experimental data. It is important to note that, for 1D-oriented samples, a distribution of the g axis system with respect to the applied magnetic field is described by a distribution of two angles. This is due to the fact that, for a given (θ, φ) position, two more independent angles, β and γ, are needed to define the position of the magnetic field with respect to the g axis system. The above treatment is identical to that of Blum (*37*) with respect to the equation for the effective g value. However, his treatment of the orientation distribution is not correct. Specifically, the assertion by Blum that a distribution of the magnetic field with respect to the film normal (distribution in θ) is equivalent to the distribution of the g tensor with respect to the film normal due to mosaic spread is incorrect.[2] In fact, as discussed above, the mosaic spread leads to a distribution in the two angles β and γ.

[2] This error has been similarly noted in ref *31* in which the distribution in θ was replaced by a distribution in β. However, this is not complete since the mosaic spread will also give rise to a distribution in γ.

Scheme 2: Schematic Representation of the Orientation of Y_D• with Respect to the Membrane[a]

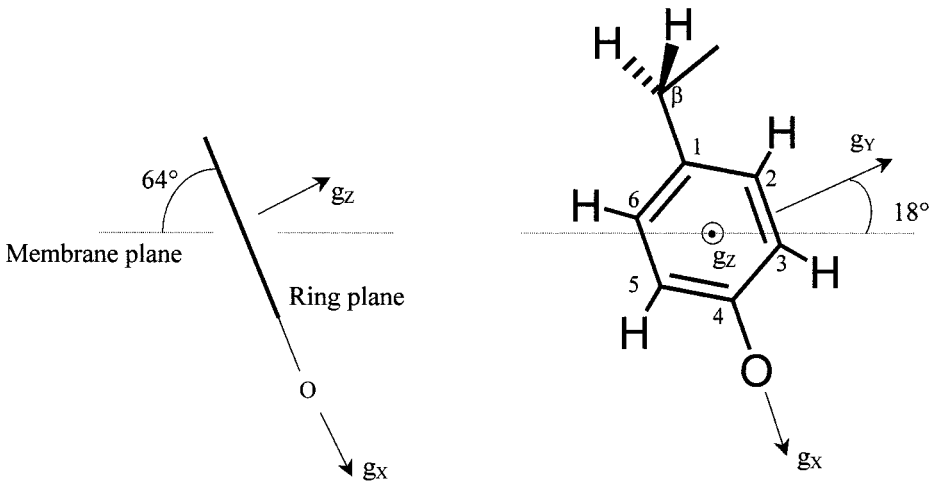

[a] Left: the membrane plane is perpendicular to the plane of the figure. Right: the tyrosine ring plane is in the plane of the figure.

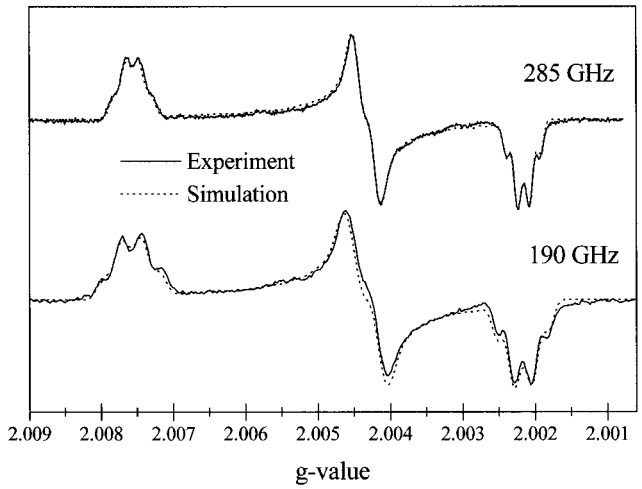

FIGURE 1: Powder spectra of Y_D• at 285 and 190 GHz. Solid line: experimental spectra. Dotted line: simulated spectra. Experimental conditions: ν_{mw} = 285.363 GHz and ν_{mw} = 190.060 GHz, respectively, modulation amplitude 0.33 mT for both spectra, and temperature 4.2 K. Simulation parameters as listed in Table 1.

Table 1: Parameters Used for the Calculation of the Powder EPR Spectrum of Y_D•

g values[a]	$g_x = 2.00756$	$g_y = 2.00432$	$g_z = 2.00215$
hyperfine values[b] (MHz)	A_x	A_y	A_z
A 3,5	24	3	19
$A\,\beta_1$	7	9	3
$A\,\beta_2$	31	28	27
A_{iso} 2,6 (fixed)	5	5	5

[a] A Gaussian distribution of 3.6×10^{-5} half-width at half-maximum for g_x was used to account for the small *g* strain observed. [b] The error in the fitted hyperfine parameters is estimated to be on the order of 5 MHz (0.1−0.2 mT). The angle between A_x and g_x for the 3 and 5 ring protons is 26°. For the two β protons the hyperfine tensor is assumed to be collinear to the *g* tensor.

RESULTS

Tyrosine D. The EPR powder pattern spectra obtained for the tyrosyl D radical at 190 and 285 GHz are shown in Figure 1. The spectra were recorded with low modulation amplitude to resolve the hyperfine couplings. The calculated spectra are shown along with the experimental data. For the simulations, the three *g* values and the anisotropic hyperfine couplings of the 3, 5 and the two β protons (see numbering in Scheme 2) were allowed to vary. The angle between the direction of the 3, 5 proton hyperfine component A_x and the g_x direction was also a variable parameter. The directions of the $A_{z\,3,5}$ and g_z components were assumed to be parallel. The hyperfine tensor for the two β-protons was assumed to be collinear to the *g* tensor. A small fixed isotropic coupling of 5 MHz was also included for each of the 2 and 6 ring protons. The final parameters yielding the best fits are shown in Table 1. A detailed comparison of the experimental 190 and 285 GHz spectra plotted with respect to the magnetic field shows an identical resolution for the g_z edge (see Figure 2). By comparison, the g_x edge exhibits a slight loss of resolution at 285 GHz relative to 190 GHz. Better simulations were obtained when the g_x value was distributed by using a Gaussian function with a half-width of 3.6×10^{-5} in *g*. Fit parameters obtained for the 285 GHz spectrum also yielded a simulation which is in very good agreement with the 190 GHz data (see Figure 2).

The experimental spectra obtained for oriented Mn-depleted PS II membranes are shown in Figure 3 along with the simulations. When the magnetic field is perpendicular to the membrane plane, the *g* value of the predominant signal is close to the g_x value; this indicates that the g_x direction is almost perpendicular to the membrane plane. The experimental spectra for both parallel and perpendicular orientations were fitted simultaneously by using the *g* values obtained from the frozen solution and the known angle between the applied magnetic field and the plastic layers. The fitting parameters were the Euler angles defining the orientation of the molecular frame (*g* frame) with respect to the intermediate frame associated with the plastic film. The orientation of the *g* tensor with respect to the molecule is known for a tyrosyl radical (*38*). The g_z axis is perpendicular to the phenyl ring. The g_x direction corresponds to the carbonyl C−O axis. The g_y direction is orthogonal to the g_x direction in the phenyl ring plane. The best fits to the experimental data were obtained for the Euler angles 64° and 18° (see Scheme 2). The phenyl ring plane makes an angle of 64° ± 5° with the membrane plane. Similar results were obtained for oxygen-evolving preparations (*30b*).

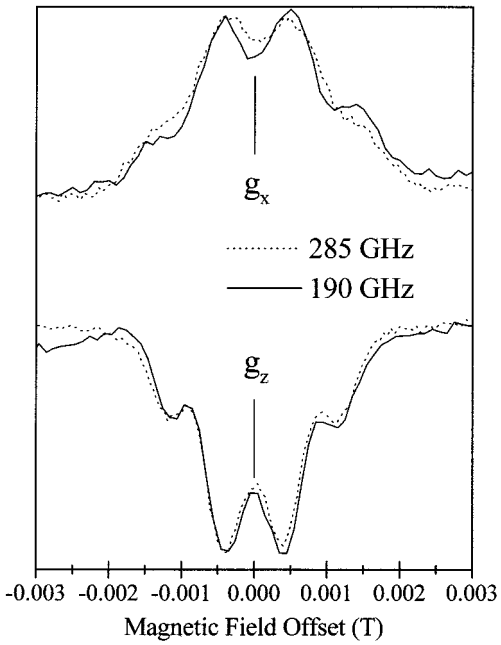

FIGURE 2: g_x and g_z edges of the experimental spectra at 285 (dotted line) and 190 GHz (solid line). Experimental conditions as in Figure 1. The apparent resolution of the g_z region at both frequencies is identical. By comparison, the resolution of the g_x region of the 285 GHz spectrum is slightly lower than that of the 190 GHz spectrum, indicating the presence of g strain.

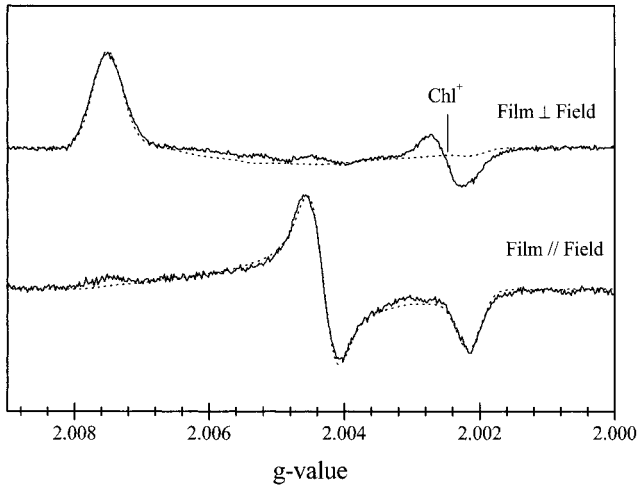

FIGURE 3: High-field EPR spectra of $Y_D^{\bullet}$ in oriented PS II membranes. Solid line: experimental spectra. Dotted line: simulated spectra. Experimental conditions: (film $\perp$ field) $\nu_{mw} = 284.804$ GHz, modulation amplitude 2.0 mT, and temperature 4.2 K; (film || field) $\nu_{mw} = 284.940$ GHz, modulation amplitude 2.0 mT, and temperature 4.2 K. Simulation parameters: g values as in Table 1, $\beta = 64°$ (distribution 20°), $\gamma = 18°$ (distribution 20°), and $\theta = 0°$ (film $\perp$ field) and 90° (film || field), respectively.

When the field direction is orthogonal to the plastic films, a single derivative line is expected (see Figure 3[3]). This is not observed experimentally. To account for the observed line shapes, a distribution in two Euler angles, β and γ, needed to be included. The half-width at half-maximum of the distribution required to correctly fit the data for the tyrosyl radical was found to be 20° for both angles.

[3] This figure differs from Figure 4 of ref *30b* in which a small distribution in θ was mistakenly used to generate the calculated spectra.

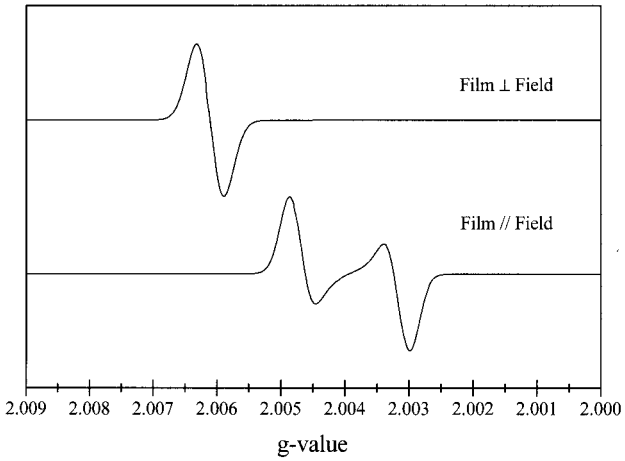

FIGURE 4: Calculated EPR spectra for $Y_D^{\bullet}$ in perfectly oriented membranes. Simulation parameters as in Figure 3 except no distribution was used for β and γ.

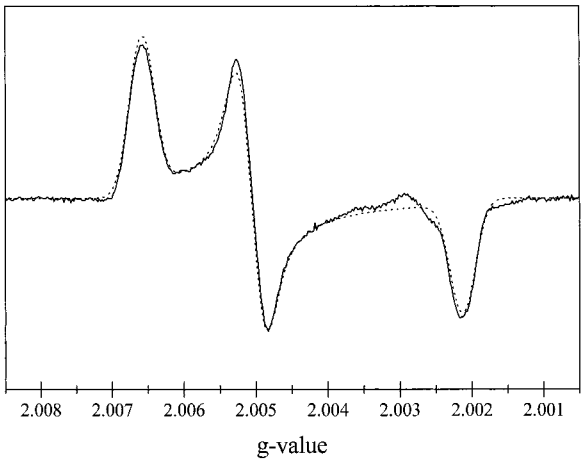

FIGURE 5: Powder spectrum of $Q_A^{\bullet-}$ at 285 GHz. Solid line: experimental spectrum. Dotted line: simulated spectrum. Experimental conditions: $\nu_{mw} = 285.090$ GHz, modulation amplitude 2.0 mT, and temperature 4.2 K. Simulation parameters: $g_x = 2.00661$, $g_y = 2.00506$, and $g_z = 2.00215$.

Plastosemiquinone Q_A. Figure 5 shows the EPR spectrum obtained at 285 GHz for a pH 9.0 frozen solution of iron-depleted PS II containing the $Q_A^{\bullet-}$ anion radical. The principal g values obtained by simulating the powder spectrum are 2.00661, 2.00506, and 2.00215 for g_x, g_y, and g_z, respectively. These values are consistent with values reported in the literature for similar anion semiquinone radical (*34*, *39*). Similar to the 9 GHz spectrum, the hyperfine coupling is unresolved and contributes only to the line width of the signal. The orientation of the g tensor with respect to the molecule is similar to that of a tyrosyl radical (*34*). The g_x axis goes through the carbonyl C−O bonds, the g_y axis is orthogonal to the g_x axis in the quinone ring plane, and the g_z axis is perpendicular to the quinone ring plane.

The spectra obtained for oriented samples of iron-depleted PS II containing the $Q_A^{\bullet-}$ anion radical are shown in Figure 6. For the orientation that corresponds to the applied magnetic field being perpendicular to the plastic film plane, one signal is observed at the value of g_y. In the other orientation where the applied magnetic field is parallel to the plastic film plane, two features at the g_x and g_z edges are observed. The combination of these results indicates that the g_y direction

Scheme 3: Schematic Representation of the Orientation of $Q_A^{\bullet-}$ with Respect to the Membrane[a]

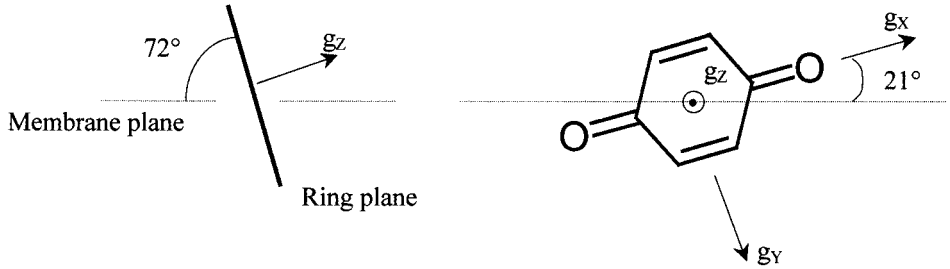

[a] Left: the membrane plane is perpendicular to the plane of the figure. Right: the quinone ring plane is in the plane of the figure.

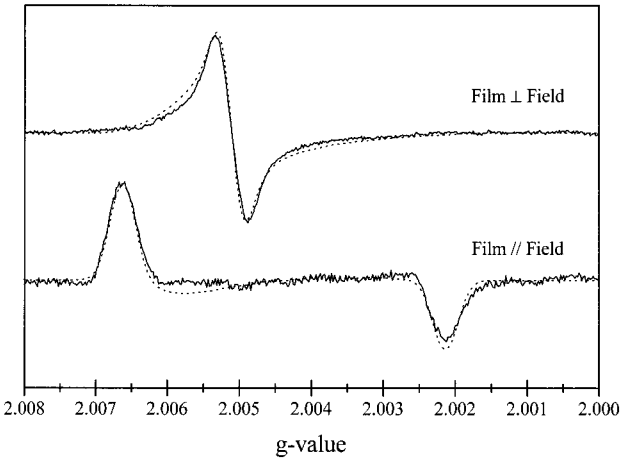

FIGURE 6: High-field EPR spectra of $Q_A^{\bullet-}$ in oriented PS II membranes. Solid line: experimental spectra. Dotted line: simulated spectra. Experimental conditions: $\nu_{mw} = 285.636$ GHz, modulation amplitude 2.0 mT, and temperature 4.2 K. Simulation parameters: g values as in Figure 5, $\beta = 72°$ (distribution 20°), $\gamma = 111°$ (distribution 20°), and $\theta = 0°$ (film ⊥ field) and 90° (film || field), respectively.

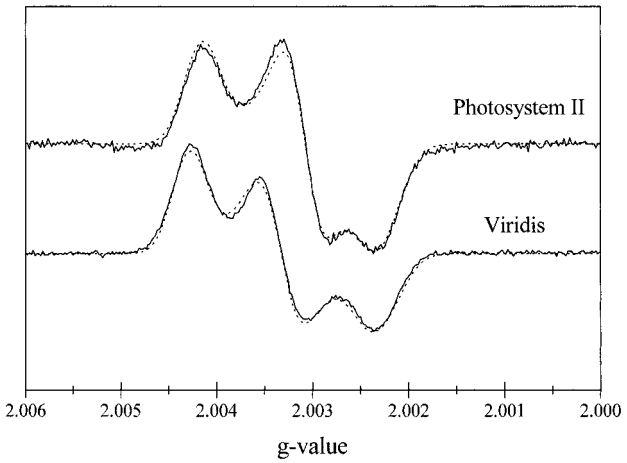

FIGURE 7: High-field powder spectra of $Pheo^{\bullet-}$ in PS II and $BPheo^{\bullet-}$ in *R. viridis* at 285 GHz. Solid line: experimental spectra. Dotted line: simulated spectra. Experimental conditions: (PS II) $\nu_{mw} = 285.090$ GHz, modulation amplitude 2.0 mT, and temperature 4.2 K; (*R. viridis*) $\nu_{mw} = 285.090$ GHz, modulation amplitude 1.0 mT, and temperature 4.2 K. Simulation parameters: (PS II) $g_x = 2.00424$, $g_y = 2.00316$, and $g_z = 2.00237$; (*R. viridis*) $g_x = 2.00437$, $g_y = 2.00340$, and $g_z = 2.00239$.

is nearly perpendicular to the membrane plane. The calculated spectra for the oriented data are plotted in Figure 6. The best fits were obtained for Euler angles of 72° and 111° and a Gaussian distribution of 20° for both angles. The quinone ring plane is oriented at 72° ± 5° to the membrane plane, and the quinone O−O axis is tilted by 21° ± 5° in the quinone ring plane compared to the membrane plane (see Scheme 3). Similar results were obtained in CN^--treated preparations (data not shown).

Pheophytin $Pheo_A$. Under strongly reducing conditions, the pheophytin anion can be accumulated when the quinone Q_A is doubly reduced. The 285 GHz EPR spectrum obtained in frozen solution for the pheophytin *a* anion in PS II is shown in Figure 7. The small g anisotropy of this radical can be resolved at this high frequency. The simulated spectrum is plotted with the experimental spectrum. The g values obtained from the fit are 2.00424, 2.00316, and 2.00237 for g_x, g_y, and g_z, respectively. For comparison, we also recorded the 285 GHz EPR spectrum of the bacteriopheophytin *b* anion radical obtained in *Rhodopseudomonas viridis* (see Figure 7). The values for the bacteriopheophytin in *R. viridis* are respectively 2.00437, 2.00340, and 2.00239. The g_z values were the same in both types of reaction center. However, the g_x and g_y values were shifted to higher field for the pheophytin in PS II compared to the bacteriopheophytin of *R. viridis*, resulting in a slightly smaller g anisotropy.

The spectra obtained for the oriented PS II samples containing the pheophytin anion radical are shown in Figure 8. The total experimental width of the spectra for oriented samples is slightly larger than that observed in the frozen solution spectrum. Hence, a slightly bigger g anisotropy than that measured for the frozen solution was required in order to properly fit the oriented data. The sample for which the

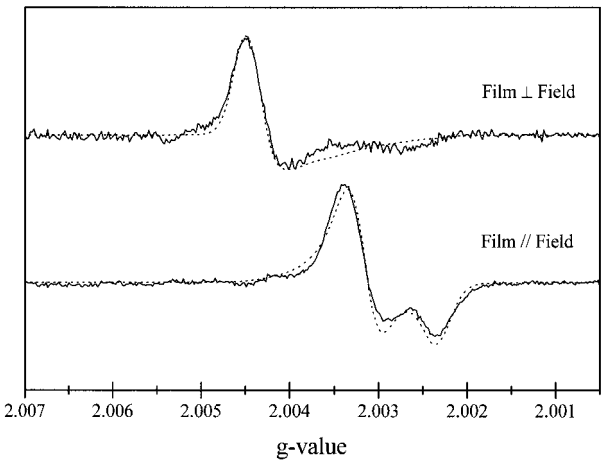

FIGURE 8: High-field EPR spectra of $Pheo^{\bullet-}$ in oriented PS II membranes. Solid line: experimental spectra. Dotted line: simulated spectra. Experimental conditions: $\nu_{mw} = 285.090$ GHz, modulation amplitude 1.4 mT, and temperature 4.2 K. Simulation parameters: $g_x = 2.00451$, $g_y = 2.00320$, $g_z = 2.00237$, $\beta = 70°$ (distribution 20°), $\gamma = 2°$ (distribution 20°), and $\theta = 0°$ (film ⊥ field) and 90° (film || field), respectively.

Scheme 4: Schematic Representation of the Orientation of the *g* Tensor of the Pheophytin Anion in PS II with Respect to the Membrane[a]

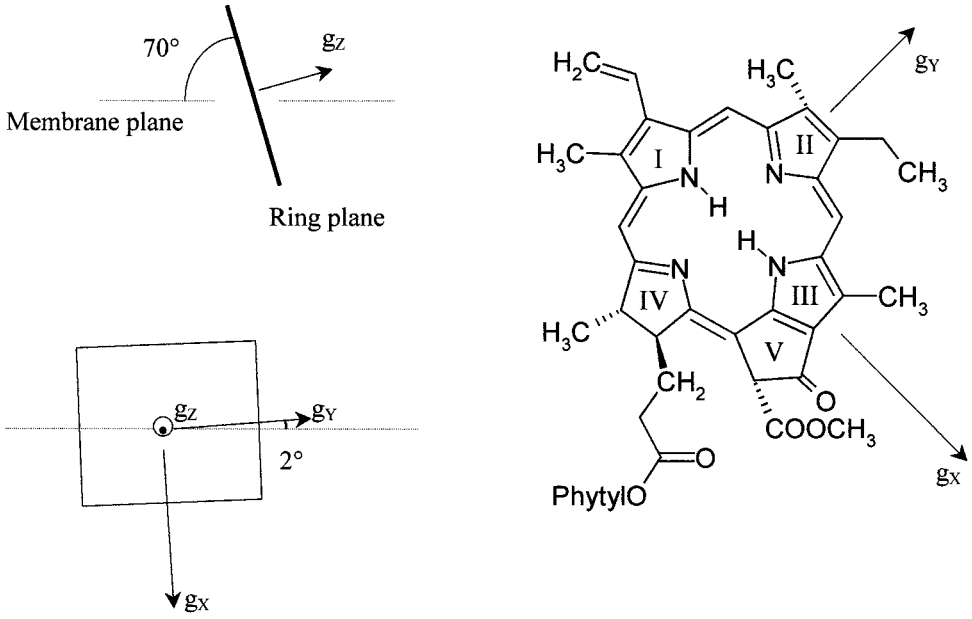

[a]Left top: the membrane plane is perpendicular to the plane of the figure. Left bottom: the pheophytin ring plane is in the plane of the figure. Right: the position of the principal *g* axis with respect to the molecule is shown. See text for details on the assignment.

magnetic field is orthogonal to the plastic film plane shows a predominant signal at a value close to the g_x value. Furthermore, from theoretical considerations (*40*), the g_z axis should be nearly perpendicular to the ring plane, resulting in an orientation for which the plane of the pheophytin is close to perpendicular to the membrane plane with the g_x direction nearly vertical. Since, for pheophytin radicals, the position of the g_x and g_y axes in the plane of the molecule is not known, it is not possible to obtain any more structural information. The Euler angles obtained from the simulations are 70° and 2°, resulting in the pheophytin plane making an angle of 70° ± 5° with respect to the membrane plane (see Scheme 4). Similar to the tyrosyl and the semiquinone radicals, the distribution was 20° for both angles.

DISCUSSION

The powder spectra of the stable tyrosyl radical, $Y_D^{\bullet}$, have been recorded at 285 and 190 GHz in frozen solution. From these two spectra, it is possible to determine the *g* values and hyperfine coupling constants. The values obtained from the simulations are listed in Table 1. The *g* values are consistent with previous measurements (*41*, *42*). The hyperfine values obtained from the high-field EPR spectra are in good agreement with those measured by 9 GHz ENDOR (*43*, *44*) and ESEEM (*45*) and a previous high-field EPR study.[4]

The g_x edge of the tyrosyl radical has been shown to be sensitive to the electrostatic environment (*46*, *47*). The g_x edge broadens very slightly with increasing magnetic field as can be seen by the modest loss in hyperfine resolution (see Figure 2). The fact that this broadening is very slight indicates the virtual absence of distribution in the electrostatic environment of the tyrosyl radical. This observation indicates that the radical is rigidly positioned and is consistent with previous ESEEM studies (*45*). Therefore, the large distribution in Euler angles found in the oriented spectra cannot be due to disorder of the tyrosyl radical within the protein.

The alternative explanation for the large distribution in Euler angles is that it is due to mosaic spread: that is, the disorder of the membrane normal with respect to the plastic film plane. Significantly, it was found that the distribution required to correctly simulate the data for the orientation of the semiquinone and the pheophytin anion was the same as for $Y_D^{\bullet}$. This also supports the attribution of the disorder to mosaic spread rather than to a disorder of the radical within the protein. The width at half-maximum of the Gaussian distribution of the Euler angles is rather large. This, however, does not prevent an accurate determination of the angular orientation of the radicals. Spectra, which were simulated by using the same distribution width but with one of the Euler angles shifted by 10°, differed significantly and failed to accurately reproduce the experimental data (*30b*). Hence we believe the error in the angles defining the orientation of the radicals to be less than 10°, and the values reported for the angles are given plus or minus 5°. Finally, it must be emphasized that, in a generalized rigorous treatment of EPR data for oriented samples, the mosaic spread must be modeled by a distribution over *both* angles defining the orientation of the *g* tensor in the IRF. In the simulations shown in this work, no distribution in θ was used.

As with tyrosyl radicals, the *g* values of semiquinone have been shown to be extremely sensitive to the local electrostatic environment (*34*, *39*). The *g* values measured for $Q_A^{\bullet -}$ are in the range of the experimental (*34*) and calculated (*39*) values obtained for model plastoquinones. However, the total *g* anisotropy ($g_x - g_z$) is higher for the plastosemiquinone in PS II compare to that measured for the radical in frozen 2-propanol solution (*34*). This indicates that the electrostatic

[4] It should be noted that the spectra we report exhibit true absorption line shape in comparison to a previous high-field study (*42*) which explored the dispersion line shape.

environment for the radical in the protein is more electroneutral than in the 2-propanol glass. This conclusion is especially interesting in light of ESEEM experiments that indicate the proximity of nitrogens reflecting potential hydrogen bond donors (*48*). Such hydrogen bond donors would contribute an electropositive environment. Therefore, these donors are either weaker than those in 2-propanol or other electronegative contributions offset those of hydrogen bonds.

By using high-field EPR in this work, the orientation of the ring plane and the O−O axis of the semiquinone has been determined. This represents important information for structural models of the PS II reaction center. The acceptor side of PS II has often been compared with that of purple bacteria reaction centers and is thought to be structurally related (*18*). It is thus of interest to compare the orientation of the semiquinone in PS II with respect to the orientation of Q_A in purple bacteria reaction centers. We used the coordinates from the crystallographic structures of the reaction centers from *R. viridis* (*49*) and *Rhodobacter sphaeroides* (*50*) to calculate the Euler angles defining the orientation of Q_A in these cases. For these calculations, the normal of the membrane plane was taken as the line joining the non-heme iron to the center of the line joining the two magnesium ions from the special pair. The resulting angle between the membrane plane and the ring of the quinone molecule was 76° for *R. sphaeroides* and 75° for *R. viridis*. This is very close to the 72° angle found here for the plastosemiquinone in PS II. It is also similar to the 76° angle measured for the phyllosemiquinone A_1 in PS I (*51*, *52*). Hence, for all three types of photosystem, the plane of the quinone has the same orientation with respect to the membrane plane. However, the tilt angle between the O−O axis and the intersection of the membrane plane with the quinone plane varies from one system to the other. In *R. sphaeroides* and *R. viridis*, this angle is small, being 15° and 4°, respectively, which makes the O−O axis almost parallel to the membrane plane. In the case of PS II the tilt angle is slightly higher with a value of 21°, while this angle is 63° in PS I (*51*, *52*). In purple bacteria, Q_A is hydrogen bonded on each of its carbonyl oxygens. One hydrogen bond is provided by a histidine which also coordinates the iron and the other hydrogen bond is provided by a protein backbone nitrogen. This has been proposed also to be the case for PS II based on ESEEM studies (*48*, *53*). The change in the tilt angle for the O−O axis of the semiquinone is small between PS II and the bacterial reaction centers. Differences could be due to the fact that we measured the orientation of the semiquinone radical with EPR whereas it is the orientation of the quinone that is given by the X-ray data. Another possible reason is that the measure for the orientation of the semiquinone was carried out on iron-depleted centers. However, experiments done on CN^--treated samples in which the iron is present yielded similar results for the orientation of the semiquinone (data not shown).

The *g* anisotropy of the pheophytin *a* and bacteriopheophytin *b* anions is smaller than that of Q_A but is still clearly resolvable. Stone has shown (*40*) that the dominant contribution to *g* anisotropy in organic radicals is due to spin−orbit coupling. Furthermore, this contribution is approximately a weighted sum of the constituent atoms (or groups of atoms). The weights depend on the ground-state spin density, atomic spin−orbit coupling constants, and terms which describe the excited states of the molecule. For π-radicals with low-lying nonbonding excited states, these last terms will significantly enhance the spin−orbit coupling contribution (*40*). This is expected for pheophytin radicals. Furthermore, for pheophytin radicals, the spin density is expected to be localized on nonprotonated nitrogens and carbonyl oxygens (*54*). These atoms also have large spin−orbit coupling constants compared to carbon. Taken together, these three contributions more than adequately account for the observed *g* anisotropy. There are two possible explanations for the small but measurable difference observed for the plant and bacterial pheophytins. The trivial one is that the intrinsic structural differences induce enough difference in the electronic structure. The second explanation is based on the observation that appreciable spin density resides on the ring V carbonyl oxygen (*54*), and the energy of the nonbonding orbitals localized on this carbonyl will be sensitive to the local protein environment. Therefore, the observed differences may be more of a reflection of the local protein electrostatic environment than a result of internal structural differences. This sensitivity to the local environment in conjunction with photoaccumulation of the pheophytin radical when the sample is dry could explain the small difference in *g* anisotropy observed for the oriented samples compare to the frozen solution data.

The angle of 70° ± 5° between the ring plane and the membrane plane measured in PS II for the pheophytin *a* is comparable with those calculated from the crystallographic data in *R. sphaeroides* and *R. viridis* (67° and 65°, respectively). This result is in agreement with the linear dichroism study of Ganago et al. (*55*), who concluded that the pheophytin ring was nearly perpendicular to the membrane plane. The tilt angle of 2° ± 5° measured in PS II gives the position of the g_x and g_y axis in the ring plane. If we assume that the ring position is similar in PS II and purple bacteria reaction centers, we can tentatively assign the g_x and g_y directions with respect to the molecule by combining the X-ray data with the measured Euler angles. The g_x axis appears to go through the protonated nitrogens of rings I and III (see Scheme 4). This direction also coincides with the ring V carbonyl bond direction, similar to tyrosyl and semiquinone radicals. This would be consistent with a relatively large spin−orbit contribution of the ring V carbonyl oxygen to the *g* anisotropy as discussed above. The g_y axis is perpendicular to g_x in the plane of the molecule and goes through the nonprotonated nitrogens of rings II and IV. Ring II is unsaturated in pheophytin *a* compared to bacteriopheophytin *b*; this is likely to induce small geometrical changes for the nitrogen of the ring that could account in part for the bigger change observed in the g_y value compared to the g_x value between the two types of radicals.

CONCLUSION

The present data, using high-field EPR and oriented multilayers, provide more information to add to the structural model of PS II. For Q_A and Pheo the data confirm the view that PS II has a close structural similarity to the purple bacteria reaction center. These data replace the assumption based on comparative and evolutionary thinking with experimentally measured structural information.

ACKNOWLEDGMENT

The authors acknowledge Yiannis Deligiannakis for earlier work on the semiquinone anion radical of PS II. We thank Jonathan Hanley for help with preparation of the oriented samples in the beginning of this work and Professor Thomas Prisner for providing the Mn/MgO sample used for the calibration of the magnet in high-field EPR experiments.

REFERENCES

1. Debus, R. J. (1992) *Biochim. Biophys. Acta 1102*, 269.
2. Rutherford, A. W., Zimmermann, J.-L., and Boussac, A. (1992) in *The Photosystems: Structure, Function and Molecular Biology* (Barber, J., Ed.) Chapter 5, Elsevier, Amsterdam, The Netherlands.
3. Britt, R. D. (1996) in *Oxygenic Photosynthesis: The Light Reactions* (Ort, D. R., and Yocum, C. F., Eds.) pp 137−164, Kluwer Academic Publishers, Dordrecht, The Netherlands.
4. Diner, B. A., and Babcock, G. T. (1996) in *Oxygenic Photosynthesis: The Light Reactions* (Ort, D. R., and Yocum, C. F., Eds.) pp 213−247, Kluwer Academic Publishers, Dordrecht, The Netherlands.
5. Klimov, V. V., Dolan, E., Shaw, E. R., and Ke, B. (1980) *Proc. Natl. Acad. Sci. U.S.A. 77*, 7227.
6. Nugent, J. H. A., Diner, B. A., and Evans, M. C. W. (1981) *FEBS Lett. 124*, 241.
7. Rutherford, A. W., and Zimmermann, J.-L. (1984) *Biochim. Biophys. Acta 767*, 168.
8. Deligiannakis, Y., Jegerschöld, C., and Rutherford, A. W. (1997) *Chem. Phys. Lett. 270*, 564.
9. Sanakis, Y., Petrouleas, V., and Diner, B. A. (1994) *Biochemistry 33*, 9922.
10. Astashkin, A. V., Kawamori, A., Kodera, Y., Kuroiwa, S., and Akabori, K. (1995) *J. Chem. Phys. 102*, 5583.
11. MacMillan, F., Lendzian, F., Renger, G., and Lubitz, W. (1995) *Biochemistry 34*, 8144.
12. Van Mieghem, F. J. E., Nitschke, W., Mathis, P., and Rutherford, A. W. (1989) *Biochim. Biophys. Acta 977*, 207.
13. Klimov, V. V., Klevanic, A. V., Shuvalov, V. A., and Krasnovsky, A. A. (1977) *FEBS Lett. 82*, 183.
14. Rutherford, A. W., and Mathis, P. (1983) *FEBS Lett. 154*, 328.
15. Deligiannakis, Y., and Rutherford, A. W. (1996) *Biochemistry 35*, 11239.
16. Koulougliotis, D., Tang, X.-S., Diner, B. A., and Brudvig, G. W. (1995) *Biochemistry 34*, 2850.
17. Ree, K.-H., Morris, E. P., Barber, J., and Kühlbrandt, W. (1998) *Nature 396*, 283.
18. Rutherford, A. W. (1989) *Trends Biochem. Sci. 14*, 227.
19. Michel, H., and Deisenhofer, J. (1988) *Biochemistry 27*, 1.
20. Debus, R. J., Barry, B. A., Babcock, G. T., and McIntosh, L. (1988) *Proc. Natl. Acad. Sci. U.S.A. 85*, 427.
21. Vermaas, W. F. J., Rutherford, A. W., and Hansson, Ö. (1988) *Proc. Natl. Acad. Sci. U.S.A. 85*, 8477.
22. (a) Tang, X.-S., and Satoh, K. (1985) *FEBS Lett. 179*, 60. (b) Yamada, Y., Tang, X.-S., Itoh, S., and Satoh, K. (1987) *Biochim. Biophys. Acta 891*, 129.
23. Svensson, B., Vass, I., Cedergren, E., and Styring, S. (1990) *EMBO J. 9*, 2051.
24. Ruffle, S. V., Donnelly, D., Blundell, T. L., and Nugent, J. H. A. (1992) *Photosynth. Res. 34*, 287.
25. Rutherford, A. W. (1985) *Biochim. Biophys. Acta 807*, 189.
26. Kurshev, V. V., Raitsimring, A. M., and Tsvetkov, Y. D. (1989) *J. Magn. Reson. 81*, 441.
27. Zech, S. G., Kurreck, J., Eckert, H. J., Renger, G., Lubitz, W., and Bittl, R. (1997) *FEBS Lett. 414*, 454.
28. Hara, H., Dzuba, S. A., Kawamori, A., Akabori, K., Tomo, T., Satoh, K., Iwaki, M., and Itoh, S. (1997) *Biochim. Biophys. Acta 1322*, 77.
29. Yoshii, T., Kawamori, A., Tonaka, M., and Akabori, K. (1999) *Biochim. Biophys. Acta 1413*, 43.
30. (a) Un, S., Brunel, L.-C., Brill, T. M., Zimmermann, J.-L., and Rutherford, A. W. (1994) *Proc. Natl. Acad. Sci. U.S.A. 91*, 5262. (b) Dorlet, P., Hanley, J., Rutherford, A. W., and Un, S. (1998) in *Photosynthesis: Mechanisms and Effects* (Garab, G., Ed.) Vol. II, pp 1395−1398, Kluwer Academic publishers, Dordrecht, The Netherlands.
31. Lakshmi, K. V., Eaton, S. S., Eaton, G. R., and Brudvig, G. W. (1999) *Biochemistry 38*, 12758.
32. (a) Berthold, D. A., Babcock, G. T., and Yocum, C. F. (1981) *FEBS Lett. 134*, 231. (b) Ford, R. C., and Evans, M. C. W. (1983) *FEBS Lett. 160*, 159.
33. Muller, F., Hopkins, M. A., Coron, N., Grynberg, M., Brunel, L. C., and Martinez, G. (1989) *Rev. Sci. Instrum. 60*, 3681.
34. Burghaus, O., Plato, M., Rohrer, M., Möbius, K., MacMillan, F., and Lubitz, W. (1993) *J. Phys. Chem. 97*, 7639.
35. Press, W. H., Flannery, B. P., Teukolsky, S. A., and Vetterling, W. T. (1986) in *Numerical Recipes*, Cambridge University Press, New York.
36. Rose, M. E. (1967) in *Elementary Theory of Angular Momentum*, Wiley, New York.
37. Blum, H., Salerno, J. C., and Leigh, J. S., Jr. (1978) *J. Magn. Reson. 30*, 385.
38. Fasanella, E. L., and Gordy, W. (1969) *Proc. Natl. Acad. Sci. U.S.A. 62*, 299.
39. Knüpling, M., Törring, J. T., and Un, S. (1997) *Chem. Phys. 219*, 291.
40. (a) Stone, A. J. (1963) *Proc. R. Soc. London, Ser. A, 271*, 424. (b) Stone, A. J. (1963) *Mol. Phys. 6*, 509. (c) Stone, A. J. (1964) *Mol. Phys. 7*, 311.
41. Un, S., Tang, X.-S., and Diner, B. A. (1996) *Biochemistry 35*, 679.
42. Farrar, C. T., Gerfen, G. J., Griffin R. G., Force, D. A., and Britt, R. D. (1997) *J. Phys. Chem. B 101*, 6634.
43. Hoganson, C. W., and Babcock, G. T. (1992) *Biochemistry 31*, 11874.
44. Rigby, S. E. J., Nugent, J. H. A., and O'Malley, P. J. (1994) *Biochemistry 33*, 1734.
45. Warncke, K., Babcock, G. T., and McCracken, J. (1994) *J. Am. Chem. Soc. 116*, 7332.
46. Un, S., Atta, M., Fontecave, M., and Rutherford, A. W. (1995) *J. Am. Chem. Soc. 117*, 10713.
47. Mezzetti, A., Maniero, A. L., Brustolon, M., and Giacometti, G. (1999) *J. Phys. Chem. A 103*, 9636.
48. Deligiannakis, Y., Hanley, J., and Rutherford, A. W. (1999) *J. Am. Chem. Soc. 121*, 7653.
49. Deisenhofer, J., Epp, O., Sinning, I., and Michel, H. (1994) PDB code 1PRC (revised 1PRCC).
50. Yeates, T. O., Komiya, H., Chirino, A., Rees, D. C., Allen, J. P., and Feher, G. (1993) PDB code 4RCR.
51. MacMillan, F., Hanley, J., van der Weerd, L., Knüpling, M., Un, S., and Rutherford, A. W. (1997) *Biochemistry 36*, 9297.
52. Kamlowski, A., Altenberg-Greulich, B., van der Est, A., Zech, S. G., Bittl, R., Fromme, P., Lubitz, W., and Stehlik, D. (1998) *J. Phys. Chem. B 102*, 8278.
53. Astashkin, A. V., Kuroiwa, S., Kawamori, A., and Akabori, K. (1998) *J. Chem. Phys. 108*, 10143.
54. (a) O'Malley, P. J. (1999) *J. Am. Chem. Soc. 121*, 3185. (b) O'Malley, P. J. (2000) *J. Phys. Chem. B 104*, 2176.
55. Ganago, I. B., Klimov, V. V., Ganago, A. O., Shuvalov, V. A., and Erokhin, Y. E. (1982) *FEBS Lett. 140*, 127.

BI000175L